

Vector Control Methods for Star-Connected Three-Phase Induction Motor Drives Under the Open-Phase Failure

M. Nikpayam¹, M. Ghanbari^{1*}, A. Esmaeli^{1,2}, M. Jannati¹

¹ Department of Electrical Engineering, Gorgan Branch, Islamic Azad University, Gorgan, Iran

² Plasma and Nuclear Fusion Research School, Nuclear Science and Technology Research Institute Tehran, Iran

Abstract- Reliability for electric motor drive systems is very vital in some industries. Selecting an appropriate control strategy for driving an electric motor during fault conditions is one of the most important issues mainly for safety-critical applications. Recently, vector control (VC) strategies have been extensively developed for star-connected three-phase induction motor drives during single-phase cut-off fault (COF) based on two different transformation matrices (TMs). Despite the effectiveness of these methods during the fault, these control systems are very complex due to their extensive on-line computation. This paper presents two simple methods based on indirect VC (IVC) and direct VC (DVC) methods for controlling a star-connected three-phase induction motor during the fault condition. The fault in this paper is limited to single-phase COF which can occur in motor stator coils. In this paper, it is shown that using a suitable TM and some changes in the control parameters, it is possible to control the faulted drive system. Performance of the proposed control methods is verified using MATLAB software and DSP/TMS320F28335 controller board for a 0.75kW star-connected three-phase induction motor drive system. The achieved results show the good performance of the introduced control systems in different operating conditions. In addition, the results demonstrate the performance of the proposed VC strategies and that of the previous works are almost the same. However, the proposed VC methods in this paper need less modification in the structure of the standard VC strategy than the previous works.

Keyword: Control of the faulted drive system, Direct and indirect vector controllers, Induction motor, Single-phase cut-off fault, Transformation matrix.

1. INTRODUCTION

Three-phase induction motors have a wide range of application in many industrial applications such as fans, wind turbines, elect vehicles, pumps, elevators, robotics, etc. Currently, more than 70% of motors utilized in industries are induction motors. These motors are the most common types of machines used in electric drive systems [1-2]. Applying electric drives in many industries is increasing. With the development of power electronic devices and microcontrollers with high-speed processing capabilities, speed control methods have also been developed on these drives. Among various control methods for electric drives, scalar control (SC), vector control (VC), direct torque control (DTC), and model predictive control (MPC) are most popular ones [3-4].

The VC method is one of the most commonly used

speed control methods due to its optimal performance in transient and steady state conditions. This method is mainly done by separating components of $d-q$ axes of the stator currents. As the result of this separation, flux and torque can be controlled independently. VC strategies can be implemented in direct and indirect ways. In the indirect VC (IVC) method, the rotor angle is obtained through the sum of the slip angle and rotor angle, while in the direct VC (DVC) method, the rotor angle is normally obtained through a sensor [4-5].

Using standard control systems for an electric motor drive system under fault conditions leads to serious damage as well as high speed and torque oscillations. On the other hand, for some industrial applications, due to the safety reasons, it is essential to control electric drives in fault conditions. The control systems which can be used for fault conditions are known as fault-tolerant control (FTC) systems. FTC systems are very important in many industries such as electric vehicles and automotive systems [6].

An electric drive system includes an electric motor, sensors, inverter, rectifier, and control system. In general, the fault in drive systems can be divided into

Received: 29 Apr. 2021

Revised: 20 May 2021

Accepted: 29 Jun. 2021

*Corresponding author:

E-mail: ghanbari@gorganiau.ac.ir (M. Ghanbari)

DOI: 10.22098/joape.2022.8802.1616

Research Paper

© 2022 University of Mohaghegh Ardabili. All rights reserved.

three categories: 1-faults on the inverter, which include open-circuit and short-circuit faults in transistor(s) [7-8], 2-faults on sensors, including electrical and mechanical faults [9-10], and 3-faults on the motor, which include faults on the rotor, stator faults, and mechanical faults [11-12]. One of the most common types of faults in three-phase induction motors is single-phase cut-off fault (COF) [11].

Different control techniques have been presented for three-phase induction motor drives under single-phase COF. In Ref. [13], induction motor performance was presented under single-phase COF based on an improved open loop v/f control. In this method, the individual harmonic voltages were injected at appropriate phase angles to neutralize the low frequency pulsating torque. The used SC method in Ref. [13] was not suitable for transient states. In Ref. [14] and [15], two approaches have been presented, respectively, for controlling a three-phase induction motor with delta connection during single-phase COF based on the magneto-motive force (MMF) calculation and using SC and VC techniques. In Ref. [16], a DVC strategy was introduced for three-phase induction motor drives with star connection under single-phase COF using a suitable transformation matrix (TM). In the proposed method in Ref. [16], two pure integrations for the rotor flux estimation were employed. Using the pure integrations led to undesired operation of the drive system at low speeds. In addition, the presented strategy in Ref. [16] was only verified by the simulation results.

In the recent years, different IVC and DVC methods have also been presented for three-phase induction motor drive systems with star connection in two-phase mode operation based on two different TMs [17-25]. For example, in Ref. [17], an IVC strategy was proposed for a star-connected three-phase induction motor under single-phase COF based on the rotor flux orientation. Although the results in this paper showed good performances of the presented IVC method during the fault, the control method suffered from the simultaneous regulation of the current PI controllers. In Ref. [18] and [23], two different IVC methods, in Ref. [20], an IVC method with rotor resistance estimation using extended Kalman filter, and in Ref. [24], an optimized IVC method using particle swarm optimization algorithm have been proposed for star-connected three-phase induction motor drives under single-phase COF. The presented strategies in Ref. [18], [20], [23], and [24] have high complexity due to using two different TMs for motor variables and depend on

motor parameters. In Refs. [19] and [21], two DVC techniques have been proposed for star-connected three-phase induction motor under single-phase COF. In these papers, an extended Kalman filter was used for rotor flux estimation. Despite the good performance of the proposed DVC systems in Refs [19] and [21] for VC of the faulty motor, in these methods, different transformation matrices should be used. These transformation matrices result in a more complicated structure and computation burden. In Ref. [22], a simple control method was proposed for VC of star-connected three-phase induction motor under single-phase COF. This method was not an accurate control model due to eliminating the backward components in the VC equations. An IVC strategy using the balanced TM for the current variables and an unbalanced TM for the voltage variables was presented in Ref. [25] for star-connected three-phase induction motor drives under the open-phase fault. Compared to the IVC methods in Ref. [18], [20], [23], and [24], the presented IVC technique in Ref. [25] had more current PI controllers. Nevertheless, the presented control strategy in Ref. [25] was more accurate after the fault. In addition to the above challenges, the presented VC methods in Ref. [17-25] are based on two different TMs, which leads to high complexity of the control system.

In this paper, two simple IVC and DVC methods are proposed for three-phase induction motor drives with star connection under single-phase COF. In the proposed methods, a TM for the stator current variables is presented. It is shown that using this TM, the motor equations in the faulty mode become similar to those of healthy induction motor equations. Therefore, it is possible to control the faulty motor with minor changes in the standard VC block diagram. In this paper, the simulation and experimental results confirm the good performance of the proposed controllers in different operating conditions. This work is organized as follows: The second section presents the used inverter topology. $d-q$ model of a three-phase induction motor with star connection under single-phase COF is presented in the third section. In the fourth section, the proposed IVC and DVC methods are discussed. The simulation and experimental results are exposed in the fifth and sixth sections and, finally, the conclusion is presented in the seventh section.

2. INVERTER TOPOLOGY

Different inverter topologies can be found in the literature to drive the faulty motor [26-27]. In this work,

suppose that the fault occurs in c-phase of the star-connected three-phase induction motor. When one of the stator phases in the motor with star connection opens, two healthy phases depend on each other. Therefore, as shown in Figure 1, the motor neutral point can be connected to the middle-point of the DC link of the inverter to rectify this dependency [28]. Figure 1 demonstrates the schematic diagram of the used inverter topology in this paper. In another topology, the motor's neutral point could be connected to the inverter fourth leg, which is less common due to high cost.

3. D-Q MODEL OF A THREE-PHASE INDUCTION MOTOR WITH STAR CONNECTION UNDER SINGLE-PHASE COF

In order to obtain the d - q model of the motor under single-phase COF, it is essential to use a suitable TM for stator components [16], [29]. Figure 2 demonstrates the d - q and magnetic axes of the stator and rotor components under single-phase COF with the availability of the induction motor neutral point. Based on Figure 2, the transformation vectors for the stator components can be expressed by Equations (1) and (2):

$$d = \begin{bmatrix} \sin \delta & \sin \left(\delta - \frac{2\pi}{3} \right) \end{bmatrix} \begin{bmatrix} f_{as} \\ f_{bs} \end{bmatrix} \quad (1)$$

$$q = \begin{bmatrix} \cos \delta & \cos \left(\delta - \frac{2\pi}{3} \right) \end{bmatrix} \begin{bmatrix} f_{as} \\ f_{bs} \end{bmatrix} \quad (2)$$

In Equations (1) and (2), f can be current, magnetic flux, etc. Based on the orthogonal principle of the transformation vectors, the angle δ can be obtained as:

$$d \cdot q^T = q \cdot d^T = 0, \quad \delta = \frac{\pi}{3} \quad (3)$$

Finally, the normalized TM for the stator components is obtained as Eq. (4) [29]:

$$[K_s^{unb}] = \frac{\sqrt{2}}{2} \begin{bmatrix} 1 & -1 \\ 1 & 1 \end{bmatrix} \quad (4)$$

The TM for the rotor components is the same to as that of the healthy state [30]:

$$[K_r^b] = \sqrt{\frac{2}{3}} \begin{bmatrix} \sin(\gamma) & \sin\left(\gamma - \frac{2\pi}{3}\right) & \sin\left(\gamma + \frac{2\pi}{3}\right) \\ \cos(\gamma) & \cos\left(\gamma - \frac{2\pi}{3}\right) & \cos\left(\gamma + \frac{2\pi}{3}\right) \end{bmatrix} \quad (5)$$

Using $[K_s^{unb}]$ and $[K_r^b]$, the following equations are obtained [29]:

$$\begin{bmatrix} V_{sd}^s \\ V_{sq}^s \\ 0 \\ 0 \end{bmatrix} = \begin{bmatrix} r_s & 0 & 0 & 0 \\ 0 & r_s & 0 & 0 \\ 0 & 0 & r_r & 0 \\ 0 & 0 & 0 & r_r \end{bmatrix} \begin{bmatrix} I_{sd}^s \\ I_{sq}^s \\ I_{rd}^s \\ I_{rq}^s \end{bmatrix} + \begin{bmatrix} 0 & 0 & 0 & 0 \\ 0 & 0 & 0 & 0 \\ 0 & 0 & 0 & -\omega_r \\ 0 & 0 & \omega_r & 0 \end{bmatrix} \begin{bmatrix} \varphi_{sd}^s \\ \varphi_{sq}^s \\ \varphi_{rd}^s \\ \varphi_{rq}^s \end{bmatrix} + P \begin{bmatrix} \varphi_{sd}^s \\ \varphi_{sq}^s \\ \varphi_{rd}^s \\ \varphi_{rq}^s \end{bmatrix} \quad (6)$$

$$\begin{bmatrix} \varphi_{sd}^s \\ \varphi_{sq}^s \\ \varphi_{rd}^s \\ \varphi_{rq}^s \end{bmatrix} = \begin{bmatrix} L_{sd} & 0 & L_d & 0 \\ 0 & L_{sq} & 0 & L_q \\ L_d & 0 & L_r & 0 \\ 0 & L_q & 0 & L_r \end{bmatrix} \begin{bmatrix} I_{sd}^s \\ I_{sq}^s \\ I_{rd}^s \\ I_{rq}^s \end{bmatrix} \quad (7)$$

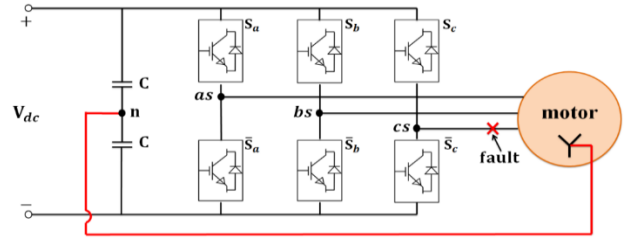


Fig. 1. Schematic diagram of the used inverter topology

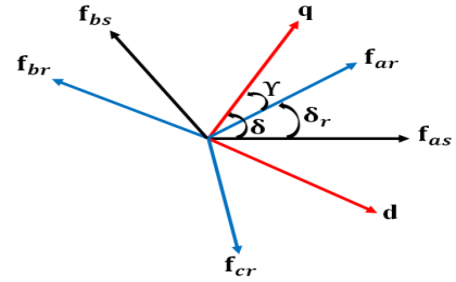


Fig. 2. d - q and magnetic axes of the stator and rotor components under single-phase COF

Consequently, the d - q model of a three-phase induction motor with star connection under single-phase COF in the stationary reference frame (SRF) is achieved as Eq. (8) [29]:

$$\begin{bmatrix} V_{sd}^s \\ V_{sq}^s \\ 0 \\ 0 \end{bmatrix} = \begin{bmatrix} r_s + L_{sd}P & 0 & L_dP & 0 \\ 0 & r_s + L_{sq}P & 0 & L_qP \\ L_dP & \omega_r L_q & r_r + L_rP & \omega_r L_r \\ -\omega_r L_d & L_qP & -\omega_r L_r & r_r + L_rP \end{bmatrix} \begin{bmatrix} I_{sd}^s \\ I_{sq}^s \\ I_{rd}^s \\ I_{rq}^s \end{bmatrix} \quad (8)$$

During single-phase COF, the electromagnetic torque equations can also be expressed by the following equations [29]:

$$M_e = \frac{\text{pole}}{2} (L_q I_{sq}^s I_{rd}^s - L_d I_{sd}^s I_{rq}^s) \quad (9)$$

$$\frac{\text{pole}}{2} (M_e - M_l) = JP\omega_r + B\omega_r \quad (10)$$

where, [29]:

$$\begin{aligned} L_{sd} &= L_{ls} + 1.5L_{ms}, L_{sq} = L_{ls} + 0.5L_{ms} \\ L_r &= L_{lr} + 1.5L_{ms}, L_d = 1.5L_{ms}, L_q = \frac{\sqrt{3}}{2}L_{ms} \end{aligned} \quad (11)$$

In these equations, V_{sd}^s , V_{sq}^s , I_{sd}^s , I_{sq}^s , φ^s , φ_{sq}^s , φ_{rd}^s , φ_{rq}^s are the voltages, currents, and fluxes of the stator and rotor d - q axes. L_{sd} , L_{sq} , L_r , L_d , L_q are the self-inductances and mutual-inductances of the stator and rotor d - q axes. Furthermore, M_e is the torque of motor, M_l is the load torque. J , ω_r , B are the moment of inertia, rotor speed, and viscous friction coefficient. Finally, $P=d/dt$.

4. VC OF A THREE-PHASE INDUCTION MOTOR UNDER SINGLE-PHASE COF

The control method based on the flux vector orientation for induction motors was developed in 1970. This method was classified into IVC and DVC. In comparison with the standard DVC methods, the standard IVC methods depend on the machine parameters. However, the standard DVC strategies have some disadvantages such as low reliability and high cost due to using flux sensor [30]. Using the TM as given in Eq. (12), the machine equations in the SRF can be written in the rotating reference frame (RRF) [30]:

$$[\mathbf{K}_s^b(\delta_e)] = [\mathbf{K}_r^b(\delta_e)] = \begin{bmatrix} \cos(\delta_e) & \sin(\delta_e) \\ -\sin(\delta_e) & \cos(\delta_e) \end{bmatrix} \quad (12)$$

In Eq. (12), δ_e is the angle between the SRF and RRF. Using Eq. (12), oscillating components are created in the faulty machine equations which produce high torque oscillations [16].

In this research, in order to control the three-phase induction motor under single-phase COF, two methods are presented using a rotational TM for the stator current variables. The proposed methods are based on IVC and DVC strategies.

4.1. Rotational TM for the stator current variables during single-phase COF

For a balanced three-phase induction motor, the stator rotating magnetic field is equal to the sum of the MMFs produced by the three stator coils. For an induction motor under single-phase COF, the total rotating MMF is the result of the sum of the MMFs generated by two healthy stator coils. In order to control a faulty machine with the non-pulsating torque, the induction motor stator MMF under single-phase COF should be equal to the stator MMF of the balanced three-phase induction motor [16]. The MMF matrix for the stator components under single-phase COF can be expressed by:

$$\begin{bmatrix} \mathbf{F}_{sd}^s \\ \mathbf{F}_{sq}^s \end{bmatrix} = \begin{bmatrix} N_{sd} & 0 \\ 0 & N_{sq} \end{bmatrix} \begin{bmatrix} \mathbf{I}_{sd}^s \\ \mathbf{I}_{sq}^s \end{bmatrix} \quad (13)$$

where F represents MMF. From Equations (12) and (13), we have:

$$\begin{bmatrix} \mathbf{K}_s^b(\delta_e) \\ \mathbf{F}_{sq}^s \end{bmatrix} \begin{bmatrix} \mathbf{F}_{sd}^s \\ \mathbf{F}_{sq}^s \end{bmatrix} = [\mathbf{K}_s^b(\delta_e)] \begin{bmatrix} N_{sd} & 0 \\ 0 & N_{sq} \end{bmatrix} \begin{bmatrix} \mathbf{I}_{sd}^s \\ \mathbf{I}_{sq}^s \end{bmatrix} = \sqrt{N_{sd}N_{sq}} \begin{bmatrix} \sqrt{\frac{N_{sd}}{N_{sq}}} \cos(\delta_e) & \sqrt{\frac{N_{sq}}{N_{sd}}} \sin(\delta_e) \\ -\sqrt{\frac{N_{sd}}{N_{sq}}} \sin(\delta_e) & \sqrt{\frac{N_{sq}}{N_{sd}}} \cos(\delta_e) \end{bmatrix} \begin{bmatrix} \mathbf{I}_{sd}^s \\ \mathbf{I}_{sq}^s \end{bmatrix} \quad (14)$$

Assuming $N_{sd}/N_{sq}=L_d/L_q$, a rotational TM for the stator current components during the faulty mode is obtained as Eq. (15):

$$\begin{bmatrix} \frac{\mathbf{F}_{sd}^e}{\sqrt{N_{sd}N_{sq}}} \\ \frac{\mathbf{F}_{sq}^e}{\sqrt{N_{sd}N_{sq}}} \end{bmatrix} = \begin{bmatrix} \mathbf{I}_{sd}^e \\ \mathbf{I}_{sq}^e \end{bmatrix} = \underbrace{\begin{bmatrix} \sqrt{\frac{L_d}{L_q}} \cos(\delta_e) & \sqrt{\frac{L_q}{L_d}} \sin(\delta_e) \\ -\sqrt{\frac{L_d}{L_q}} \sin(\delta_e) & \sqrt{\frac{L_q}{L_d}} \cos(\delta_e) \end{bmatrix}}_{[\mathbf{K}_{is}^{umb}(\delta_e)]} \begin{bmatrix} \mathbf{I}_{sd}^s \\ \mathbf{I}_{sq}^s \end{bmatrix} \quad (15)$$

4.2. IVC strategy for the induction motor during single-phase COF

Considering Eqns. (6)-(9), the rotor flux, rotor voltage, and electromagnetic torque equations in the RRF can be written as Eqns. (16)-(18):

Rotor flux equations:

$$\begin{bmatrix} \mathbf{K}_r^b(\delta_e) \\ \mathbf{K}_r^b(\delta_e) \end{bmatrix} \begin{bmatrix} \Phi_{rd}^s \\ \Phi_{rq}^s \end{bmatrix} = [\mathbf{K}_r^b(\delta_e)] \begin{bmatrix} L_d & 0 \\ 0 & L_q \end{bmatrix} [\mathbf{K}_{is}^{umb}(\delta_e)]^{-1} [\mathbf{K}_{is}^{umb}(\delta_e)] \begin{bmatrix} \mathbf{I}_{sd}^s \\ \mathbf{I}_{sq}^s \end{bmatrix} + [\mathbf{K}_r^b(\delta_e)] \begin{bmatrix} L_r & 0 \\ 0 & L_r \end{bmatrix} [\mathbf{K}_r^b(\delta_e)]^{-1} [\mathbf{K}_r^b(\delta_e)] \begin{bmatrix} \mathbf{I}_{rd}^s \\ \mathbf{I}_{rq}^s \end{bmatrix} \quad (16)$$

Rotor voltage equations:

$$\begin{bmatrix} \mathbf{K}_r^b(\delta_e) \\ \mathbf{K}_r^b(\delta_e) \end{bmatrix} \begin{bmatrix} 0 \\ 0 \end{bmatrix} = [\mathbf{K}_r^b(\delta_e)] \begin{bmatrix} L_d P & \omega_r L_q \\ -\omega_r L_d & L_q P \end{bmatrix} [\mathbf{K}_{is}^{umb}(\delta_e)]^{-1} [\mathbf{K}_{is}^{umb}(\delta_e)] \begin{bmatrix} \mathbf{I}_{sd}^s \\ \mathbf{I}_{sq}^s \end{bmatrix} + [\mathbf{K}_r^b(\delta_e)] \begin{bmatrix} r_r + L_r P & \omega_r L_r \\ -\omega_r L_r & r_r + L_r P \end{bmatrix} [\mathbf{K}_r^b(\delta_e)]^{-1} [\mathbf{K}_r^b(\delta_e)] \begin{bmatrix} \mathbf{I}_{rd}^s \\ \mathbf{I}_{rq}^s \end{bmatrix} \quad (17)$$

Electromagnetic torque equation:

$$M_e = \frac{\text{pole}}{2} (L_q I_{sq}^s I_{rd}^s - L_d I_{sd}^s I_{rq}^s) = \frac{\text{pole}}{2} \begin{bmatrix} I_{rd}^s & I_{rq}^s \\ -L_d & 0 \end{bmatrix} \begin{bmatrix} 0 & L_q \\ -L_d & 0 \end{bmatrix} \begin{bmatrix} \mathbf{I}_{sd}^s \\ \mathbf{I}_{sq}^s \end{bmatrix} = \frac{\text{pole}}{2} \begin{bmatrix} I_{rd}^s & I_{rq}^s \end{bmatrix} [\mathbf{K}_r^b(\delta_e)]^T \left([\mathbf{K}_r^b(\delta_e)]^{-1} \right)^T \begin{bmatrix} 0 & L_q \\ -L_d & 0 \end{bmatrix} [\mathbf{K}_{is}^{umb}(\delta_e)]^{-1} [\mathbf{K}_{is}^{umb}(\delta_e)] \begin{bmatrix} \mathbf{I}_{sd}^s \\ \mathbf{I}_{sq}^s \end{bmatrix} \quad (18)$$

After simplifying Eqns. (16)-(18) we have:

$$\begin{bmatrix} \Phi_{rd}^e \\ \Phi_{rq}^e \end{bmatrix} = \begin{bmatrix} \sqrt{L_d L_q} & 0 \\ 0 & \sqrt{L_d L_q} \end{bmatrix} \begin{bmatrix} \mathbf{I}_{sd}^e \\ \mathbf{I}_{sq}^e \end{bmatrix} + \begin{bmatrix} L_r & 0 \\ 0 & L_r \end{bmatrix} \begin{bmatrix} \mathbf{I}_{rd}^e \\ \mathbf{I}_{rq}^e \end{bmatrix} \quad (19)$$

$$\begin{bmatrix} 0 \\ 0 \end{bmatrix} = \begin{bmatrix} \sqrt{L_d L_q} P & -\omega_{sl} \sqrt{L_d L_q} \\ \omega_{sl} \sqrt{L_d L_q} & \sqrt{L_d L_q} P \end{bmatrix} \begin{bmatrix} \mathbf{I}_{sd}^e \\ \mathbf{I}_{sq}^e \end{bmatrix} + \begin{bmatrix} r_r + L_r P & -\omega_{sl} L_r \\ \omega_{sl} L_r & r_r + L_r P \end{bmatrix} \begin{bmatrix} \mathbf{I}_{rd}^e \\ \mathbf{I}_{rq}^e \end{bmatrix} \quad (20)$$

$$M_e = \frac{\text{pole}}{2} \sqrt{L_d L_q} (I_{sq}^e I_{rd}^e - I_{sd}^e I_{rq}^e) \quad (21)$$

where, $\omega_{sl} = \omega_e - \omega_r$. Moreover, ω_e is the angular speed in the RRF. In the RRF, d-axis is aligned with the rotor

for open-phase FTC of star-connected three-phase induction motor drives. It should be mentioned that the selection of coefficients of PI controllers has a significant effect on the drive system performance. Coefficients of PI controllers in this research are obtained based on the technique used in Ref. [25].

5. SIMULATION RESULTS

Simulation studies in the Matlab environment based on the proposed IVC and DVC techniques are performed for a 0.75kW star-connected three-phase induction motor. In the simulations, the sampling time for the control methods is set to $100\mu\text{s}$, $|\varphi_r^*| = 1\text{wb}$, and the single-phase COF happens in c-phase. Parameters of the motor are given in Table 1.

Figures 5(a) and 5(b) illustrate the performance of the proposed IVC and DVC methods during single-phase COF (Figure 5(a) shows the simulation results of the proposed IVC and Figure 5(b) represents the simulation results of the proposed DVC). In these figures, from $t=2\text{sec}$ to $t=5\text{sec}$, the reference speed is 100rpm , from $t=5\text{sec}$ to $t=7\text{sec}$, the reference speed changes from 100rpm to 300rpm , and from $t=7\text{sec}$ to $t=10\text{sec}$, the reference speed is 300rpm . Besides, in both figures, a step load torque equal to 0.7N.m is applied at $t=9\text{sec}$. These two simulations include the waveforms of the reference and real motor speeds, reference and real motor fluxes, and electromagnetic torque. As shown in Figures 5(a) and 5(b), both IVC and DVC methods are able to control the faulted motor at different speeds, even during the load condition. Speed response shows that the real rotor speed can track the reference speed. As can be seen from the rotor flux signal, the real rotor flux can follow its reference value. From the torque response, it is observed that except during the load and transient periods, the average value of the torque is zero. However, during the load condition, the average value of the torque is equal to the applied load.

6. EXPERIMENTAL RESULTS

A two-level voltage source inverter in cooperation with a star-connected three-phase induction motor is utilized to study the performance of the standard IVC strategy, presented DVC strategy in Ref. [19], and proposed VC strategies during single-phase COF. The IVC equations as well as their block diagram of the standard control strategy based on IVC are given in Appendix. The experimental rig is exposed in Figure 6.

The experimental setup consists of gate driver circuits, six IGBT components, DC power source,

0.75kW star-connected three-phase induction motor, incremental encoder for the speed measurement, current sensors, and DC generator along with a resistive load. All control strategies are programmed in PSIM software and using DSP/TMS320F28335. The sampling time for control techniques is set to $100\mu\text{s}$ and $|\varphi_r^*| = 1\text{wb}$. In the tests, single-phase COF happens in c-phase and very fast fault detection based on Ref. [25] is considered. To emulate single-phase COF, an electronic switch is used in c-phase and it is opened to realize the faulty mode. The parameters of the motor are given in Table 1.

6.1. Comparing the standard IVC strategies and the proposed DVC strategy under normal and single-phase COF conditions

Figures 7(a) and 8(a) show the experimental results of the three-phase induction motor using the standard IVC strategy. Figures 7(b) and 8(b) demonstrate the experimental results of the three-phase induction motor using the standard IVC strategy when the motor neutral point is connected to the middle-point of the DC link of the inverter. Figures 7(c) and 8(c) show the experimental results of the three-phase induction motor using the proposed DVC strategy. In Figure 7, the reference speed changes from 1200rpm to 600rpm . In addition, in Figure 8, the reference speed is 1200rpm . Figure 7 shows the speed, rotor flux, and torque signals (from top to bottom: speed, rotor flux, and torque) and Figure 8 demonstrates the faulty motor phase currents (from top to bottom: a- phase current, c-phase current, and b-phase current).

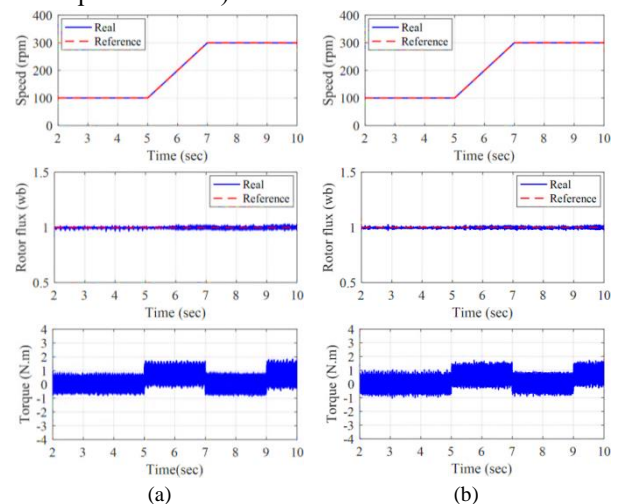


Fig. 5. Simulation results of the proposed IVC and DVC strategies during single-phase COF for different reference speeds ; (a) proposed IVC strategy, (b) proposed DVC strategy

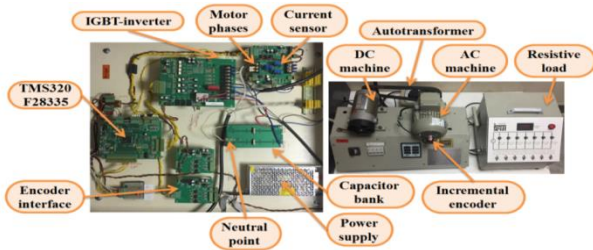


Fig. 6. Experimental rig

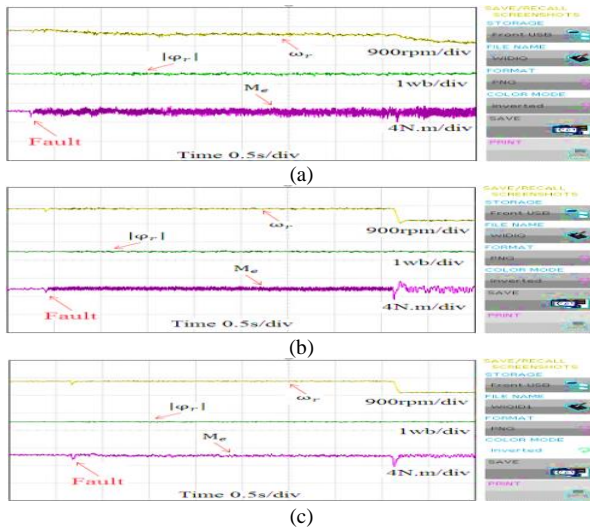


Fig. 7. Experimental results of the speed, rotor flux, and torque signals under normal and single-phase COF conditions when the reference speed changes from 1200rpm to 600rpm; (a) standard IVC strategy, (b) standard IVC strategy when the motor neutral point is connected to the middle-point of the DC link of the inverter, (c) proposed DVC strategy

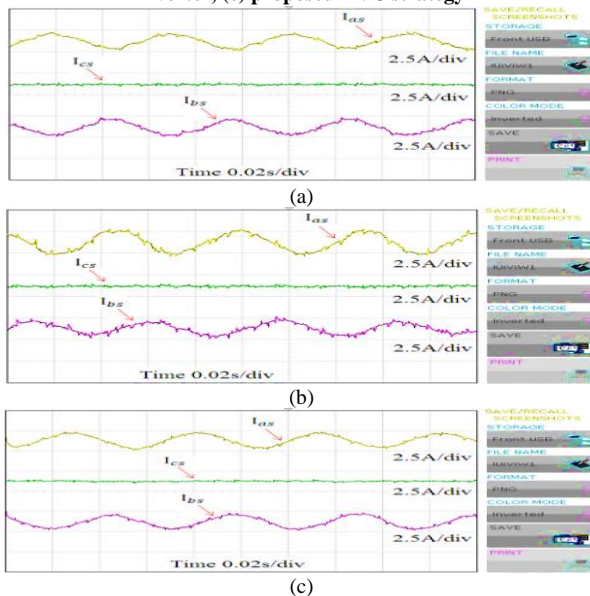


Fig. 8. Experimental results of the motor phase currents after single-phase COF condition when the reference speed is 1200rpm; (a) standard IVC strategy, (b) standard IVC strategy when the motor neutral point is connected to the middle-point of the DC link of the inverter, (c) proposed DVC strategy

As in Figures 7(a) and 7(b), there are high oscillations in waveforms of the speed and rotor flux signals after

single-phase COF. Furthermore, these oscillations are visible in the torque signal. It can also be seen that the proposed DVC system has good dynamic and steady state performance under normal and single-phase COF conditions (see Figure 7(c)). According to this figure, the proposed DVC technique is capable to control the faulted machine during different speeds. Speed response of Figure 7(c) reveals that the speed and rotor flux signals can track the reference speed and reference rotor flux, respectively. From the torque response of Figure 7(c), it is seen that except during the fault and transient periods, the average value of the torque is zero.

Figure 8(a) shows that the motor currents in the healthy phases cannot be controlled individually ($i_{as} = -i_{bs}$). Based on the presented results of Figure 8(b), the motor currents in the healthy phases lose their sinusoidal forms and are unbalanced. As shown in Figure 8(c), the motor currents in the healthy phases are balanced and sinusoidal, and can be controlled individually using the proposed DVC system.

6.2. Performance of the proposed IVC strategy under normal and single-phase COF conditions during no-load and load conditions

Figures 9(a) and 9(b) show the experimental results of the three-phase induction motor using the proposed IVC strategy under normal and single-phase COF conditions during no-load and the mechanical load equal to 1N.m. In Figure 9(a), the reference speed changes from 900rpm to 1500rpm. In addition, in Figure 9(b), the reference speed is 1500rpm. Figure 9(a) shows the speed, rotor flux, and torque signals (from top to bottom: speed, rotor flux, and torque) and Figure 9(b) shows the three-phase induction motor phase currents after the single-phase COF (from top to bottom: a-phase current, c-phase current, and b-phase current).

As shown in Figure 9, the proposed IVC method is able to control the healthy and faulty motors at different speeds without any considerable transient and steady state errors, even during the load condition. As can be seen from the speed and rotor flux signals, these signals can follow their reference values. Based on the experiment, a decrease in the motor speed is observed when the fault occurs, but the control system successfully manages the disturbance in very short time (0.1sec). From the torque response, it is observed that except during the load and transient periods, the average value of the torque is zero. In addition, during the load condition, the average value of the torque is equal to the applied load. Also, in this case, using the introduced IVC method, the motor currents after the fault and

during the load condition are balanced and have sinusoidal forms (see Figure 9(b)).

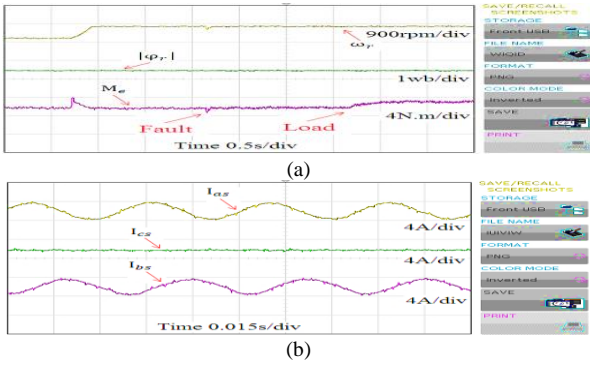


Fig. 9. Experimental results of the speed, rotor flux, torque, and motor phase currents using the proposed IVC strategy under normal and single-phase COF conditions during no-load and load conditions; (a) speed, rotor flux, and torque, (b) motor phase currents

6.3. Performance of the proposed DVC strategy under normal and single-phase COF conditions at low speed operation

Figure 10 shows the experimental results of the three-phase induction motor using the proposed DVC strategy under normal and single-phase COF conditions at low speed operation. In Figure 10(a), the reference speed changes from 100rpm to 200rpm to 100rpm. Furthermore, in Figure 10(b), the reference speed is 200rpm. Figure 10(a) shows the speed, rotor flux, and torque signals (from top to bottom: speed, rotor flux, and torque) and Figure 10(b) shows the three-phase induction motor phase currents after single-phase COF (from top to bottom: a-phase current, c-phase current, and b-phase current).

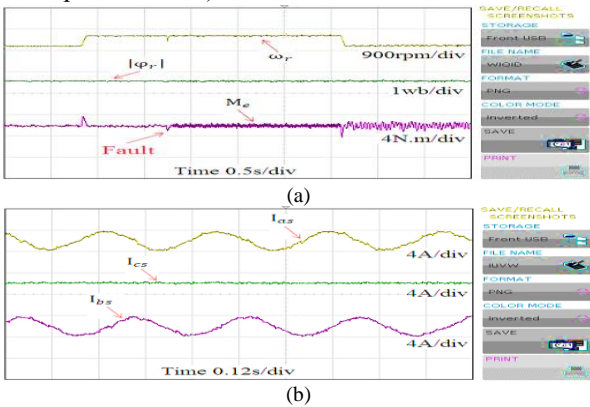


Fig. 10. Experimental results of the speed, rotor flux, torque, and motor phase currents using the proposed DVC strategy under normal and single-phase COF conditions at low speed operation; (a) speed, rotor flux, and torque, (b) motor phase currents

As represented, the proposed DVC is able to satisfactorily control the motor at low speed operation under normal and single-phase COF conditions. As shown in Figure 10(a), the speed and rotor flux of the faulty star-connected three-phase induction motor using the proposed DVC strategy can track the reference

speed and reference rotor flux, respectively. From the torque response of Figure 10(a), it is seen that torque oscillations at low speed operation are reasonable and its variations are proportional to speed variations. In this case as well, motor currents after single-phase COF are balanced and sinusoidal, as illustrated in Figure 10(b).

6.4. Comparing the presented DVC strategy in Ref. [19] and the proposed DVC strategy during single-phase COF

Fig 11 shows the experimental results of the faulty three-phase induction motor using the presented DVC strategy in Ref. [19] and the proposed DVC strategy in this paper during no-load and the mechanical load equal to 1.9N.m (100% of the maximum allowed load), respectively. In Figure 11, the reference speed is 1500rpm. Fig. 11 shows the speed and torque signals (from top to bottom: speed and torque).

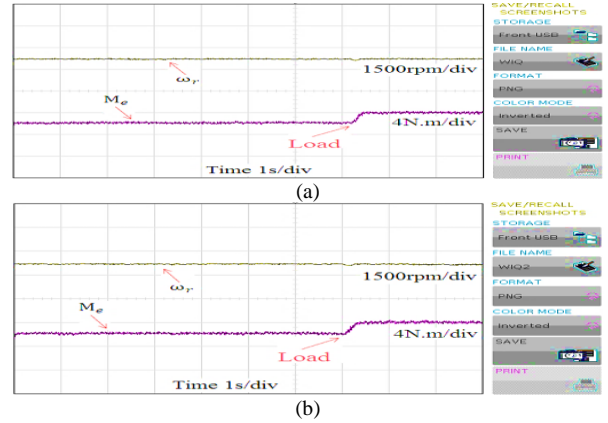


Fig. 11. Experimental results of the speed and torque signals under single-phase COF condition based on the presented DVC strategy in Ref. [19] and the proposed DVC strategy (a) presented DVC strategy in Ref. [19], (b) proposed DVC strategy

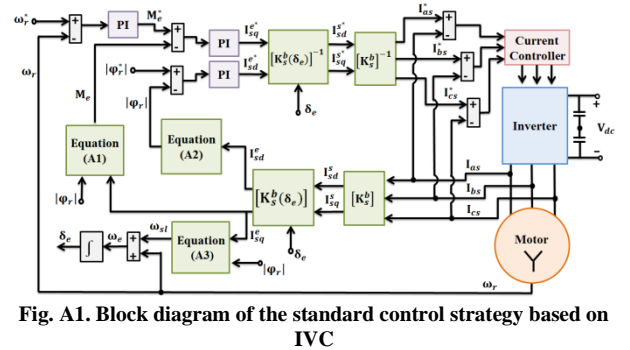


Fig. A1. Block diagram of the standard control strategy based on IVC

As can be seen in Figure 11, the presented DVC strategy in Ref. [19] and the proposed DVC strategy are able to satisfactorily track the speed during no-load and the mechanical load. In addition, the results show that the oscillations of the torque using two DVC methods are almost the same. Despite the good performance of the presented DVC strategy in Ref. [19], this method suffers from high complexity due to using different transformation matrices and extended Kalman filter

compared to the proposed DVC strategy. In this paper, two simple methods for improving reliability of vector controlled star-connected three-phase induction motor drives against single-phase COF were proposed and verified using simulations and experiments. Based on the results, the proposed control strategies offered a significant increase in the star-connected three-phase induction motor drive reliability while keeping VC dynamic and steady state performance.

7. CONCLUSION

In this paper, two simple methods were presented for IVC and DVC of a three-phase induction motor with star connection under single-phase COF. The proposed IVC and DVC methods were based on using a suitable TM for the stator current components. It was shown that with some changes in the standard control structure of the healthy induction motor drive, VC of the induction machine under single-phase COF was possible. Simulation and experimental results confirmed the good performance of the proposed VC systems in different conditions. According to the obtained results, it was observed that the proposed control methods during single-phase COF showed better dynamic and steady state performance than the standard control methods. Based on the results, the proposed control strategy in Ref. [19] and the proposed control strategy in this research produced low speed and torque oscillations. However, in the proposed control strategy in Ref. [19], different transformation matrices and an extended Kalman filter should be employed. Using different transformation matrices and extended Kalman filter increased the complexity of the drive system. As the three-phase induction motor under single-phase COF was equivalent to an asymmetrical two-phase machine with different turn numbers, the presented IVC and DVC methods in this paper were applicable for the VC of asymmetrical two-phase machines.

APPENDIX

The IVC equations for a three-phase induction motor are as Eqns. (A1)-(A3) [30]:

$$M_e = \frac{\text{pole}}{2} \frac{L_M}{L_r} I_{sq}^e |\varphi_r| \quad (\text{A1})$$

$$|\varphi_r| = \frac{L_M}{1 + \tau_r P} I_{sd}^e \quad (\text{A2})$$

$$\omega_{sl} = \frac{L_M}{\tau_r |\varphi_r|} I_{sq}^e \quad (\text{A3})$$

where, $L_M=1.5L_{ms}$ is the mutual-inductance of the three-phase induction motor. Based on Eqns. (A1)-(A3),

the block diagram of the standard IVC method for three-phase induction motor drives using the hysteresis current controller is shown in Fig. A1. In Fig. A1 [30]:

$$[K_s^b] = \sqrt{\frac{2}{3}} \begin{bmatrix} 1 & -\frac{1}{2} & -\frac{1}{2} \\ 0 & \frac{\sqrt{3}}{2} & -\frac{\sqrt{3}}{2} \end{bmatrix} \quad (\text{A4})$$

REFERENCES

- [1] H. Moayedirad, S. Nejad, "Increasing the efficiency of the power electronic converter for a proposed dual stator winding squirrel-cage induction motor drive using a five-leg inverter at low speeds", *J. Oper. Autom. Power Eng.*, vol. 6, pp. 23-39, 2018.
- [2] M. Bigdeli, D. Azizian, E. Rahimpour, "An improved big bang-big crunch algorithm for estimating three-phase induction motors efficiency", *J. Oper. Autom. Power Eng.*, vol. 4, pp. 83-92, 2016.
- [3] M. Hannan et al., "Optimization techniques to enhance the performance of induction motor drives: A review", *Renew. Sustain. Energy Rev.*, vol. 81, pp. 1611-26, 2018.
- [4] M. Jannati et al., "A review on variable speed control techniques for efficient control of single-phase induction motors: evolution, classification, comparison", *Renew. Sustain. Energy Rev.*, vol. 75, pp. 1306-19, 2017.
- [5] A. Datta, G. Poddar, "Improved low-frequency operation of hybrid inverter for medium-voltage induction motor drive under v/f and vector control mode of operation", *IEEE J. Emerg. Selected Top. Power Electron.*, vol. 8, pp. 1248-57, 2019.
- [6] M. Benbouzid, D. Diallo, M. Zeraoulia, "Advanced fault-tolerant control of induction-motor drives for EV/HEV traction applications: From conventional to modern and intelligent control techniques", *IEEE Trans. Veh. Tech.*, vol. 56, pp. 519-28, 2007.
- [7] S. Nagarajan, S. Reddy, "Digital simulation of fault tolerant inverter fed induction motor with a leg swap module", *Majlesi J. Electr. Eng.*, vol. 6, pp. 38, 2012.
- [8] R. Ribeiro et al., "Fault-tolerant voltage-fed PWM inverter AC motor drive systems", *IEEE Trans. Power Electron.*, vol. 51, pp. 439-46, 2004.
- [9] D. Delgado, D. Espinoza-Trejo, E. Palacios, "Fault-tolerant control in variable speed drives: a survey", *IET Electr. Power Appl.*, vol. 2, pp. 121-14, 2008.
- [10] A. Raisemche et al., "Two active fault-tolerant control schemes of induction-motor drive in EV or HEV", *IEEE Trans. Veh. Tech.*, vol. 63, pp. 19-29, 2014.
- [11] A. Ahmed, B. Mirafzal, N. Demerdash, "A fault tolerant technique for Δ -connected ac motor-drive systems", *IEEE Trans. Energy Conv.*, vol. 26., pp. 646-53, 2011.
- [12] S. Kim, J. Seok, "High-frequency signal injection-based rotor bar fault detection of inverter-fed induction motors with closed rotor slots", *IEEE Trans. Ind. Appl.*, vol. 47, pp. 1624-31, 2011.
- [13] D. Kastha, B. Bose, "Fault mode single-phase operation of a variable frequency induction motor drive and improvement of pulsating torque characteristics", *IEEE Trans. Ind. Electron.*, vol. 41, pp. 426-33, 1994.
- [14] A. Ahmed, N. Demerdash, "Control of open-loop PWM delta-connected motor-drive systems under one phase failure condition", *J. Power Electron.*, vol. 11, pp. 824-36, 2011.

- [15] A. Ahmed, N. Demerdash, "Fault-tolerant operation of delta-connected scalar-and vector-controlled AC motor drives", *IEEE Trans. Power Electron.*, vol. 27, pp. 3041-49, 2012.
- [16] Y. Zhao, T. Lipo, "An approach to modeling and field-oriented control of a three phase induction machine with structural unbalance", *IEEE-APEC Conf.*, 1996.
- [17] M. Jannati, N. Idris, M. Aziz, "Vector control of star-connected 3-phase induction motor drives under open-phase fault based on rotor flux field-oriented control", *Electr. Power Comp. Syst.*, vol. 44, pp. 2325-37, 2016.
- [18] M. Jannati et al., "Experimental evaluation of FOC of 3-phase IM under open-phase fault", *Int. J. Electron.*, vol. 104, pp. 1675-88, 2017.
- [19] R. Tabasian et al., "A novel direct field-oriented control strategy for fault-tolerant control of induction machine drives based on EKF", *IET Electr. Power Appl.*, 2021.
- [20] M. Jannati, N. Idris, M. Aziz, "Indirect rotor field-oriented control of fault-tolerant drive system for three-phase induction motor with rotor resistance estimation using EKF", *TELKOMNIKA Indonesian J. Electr. Eng.*, vol. 12, pp. 6633-43, 2014.
- [21] M. Nikpayam et al., "Fault-tolerant control of Y-connected three-phase induction motor drives without speed measurement", *Measurement*, vol. 149, pp. 106993, 2020.
- [22] R. Tabasian, M. Ghanbari, M. Jannati, "A simple method for vector control of 3-phase induction motor under open-phase fault for electric vehicle applications", *J. Appl. Dynamic Syst. Control*, vol. 1, pp. 1-9, 2018.
- [23] M. Jannati, N. Idris, M. Aziz, "Performance evaluation of the field-oriented control of star-connected 3-phase induction motor drives under stator winding open-circuit faults", *J. Power Electron.*, vol. 16, pp.982-93, 2016.
- [24] M. Nikpayam et al., "An optimized vector control strategy for induction machines during open-phase failure condition using particle swarm optimization algorithm", *Int. Trans. Electr. Energy Syst.*, vol. 30, pp.12669, 2020.
- [25] H. Abbasi et al., "IRFOC of induction motor drives under open-phase fault using balanced and unbalanced transformation matrices", *IEEE Trans. Ind. Electron.*, 2020.
- [26] B. Welchko et al., "Fault tolerant three-phase AC motor drive topologies: a comparison of features, cost, and limitations", *IEEE Trans. Power Electron.*, vol. 19, pp. 1108-16, 2004.
- [27] R. Tabasian et al., "Control of three-phase induction machine drives during open-circuit fault: A review", *IETE J. Res.*, 2020.
- [28] M. Tousizadeh et al., "Performance comparison of fault-tolerant three-phase induction motor drives considering current and voltage limits", *IEEE Trans. Ind. Electron.*, vol. 66, pp. 2639-48, 2018.
- [29] M. Jannati, N. Idris, Z. Salam, "A new method for modeling and vector control of unbalanced induction motors", *IEEE Energy Conv. Congr. Expos.*, 2012.
- [30] P. Vas, "Sensorless vector and direct torque control", Oxford Univ, Singapore, Mc-Graw-Hill, 1998.